Microstructural evolution and mechanical properties of pure titanium powders processed by spark plasma sintering

Glenda T. Motsi, Sophie Guillemet, Geoffroy Chevallier, Mxolisi B. Shongwe, Peter A. Olubambi, Claude Estournès

▶ **To cite this version:**

Glenda T. Motsi, Sophie Guillemet, Geoffroy Chevallier, Mxolisi B. Shongwe, Peter A. Olubambi, et al.. Microstructural evolution and mechanical properties of pure titanium powders processed by spark plasma sintering. Powder Technology, 2019, 345, pp.415-424. 10.1016/j.powtec.2019.01.005 . hal-02016028

HAL Id: hal-02016028
https://hal.science/hal-02016028

Submitted on 12 Feb 2019

HAL is a multi-disciplinary open access archive for the deposit and dissemination of scientific research documents, whether they are published or not. The documents may come from teaching and research institutions in France or abroad, or from public or private research centers.

L'archive ouverte pluridisciplinaire **HAL**, est destinée au dépôt et à la diffusion de documents scientifiques de niveau recherche, publiés ou non, émanant des établissements d'enseignement et de recherche français ou étrangers, des laboratoires publics ou privés.

OATAO
Open Archive Toulouse Archive Ouverte

Open Archive Toulouse Archive Ouverte (OATAO)

OATAO is an open access repository that collects the work of Toulouse researchers and makes it freely available over the web where possible

This is an author's version published in: **http://oatao.univ-toulouse.fr/21745**

Official URL: https://doi.org/10.1016/j.powtec.2019.01.005

To cite this version:

Motsi, Glenda T. and Guillemet, Sophie and Chevallier, Geoffroy and Shongwe, Mxolisi B. and Olubambi, Peter A. and Estournès, Claude *Microstructural evolution and mechanical properties of pure titanium powders processed by spark plasma sintering.* (2019) Powder Technology, 345. 415-424. ISSN 0032-5910

Any correspondence concerning this service should be sent to the repository administrator: tech-oatao@listes-diff.inp-toulouse.fr

Microstructural evolution and mechanical properties of pure titanium powders processed by spark plasma sintering

Glenda T. Motsi [a,b,*], Sophie Guillemet-Fritsch [a], Geoffroy Chevallier [a], Mxolisi B. Shongwe [b], Peter A. Olubambi [c], Claude Estournes [a]

[a] CIRIMAT, Université de Toulouse, CNRS, Université Toulouse 3 - Paul-Sabatier, 118 route de Narbonne, 31062 Toulouse cedex 09, France
[b] Tshwane University of Technology, Department of Chemical, Metallurgical and Materials Engineering, Pretoria, South Africa
[c] University of Johannesburg, School of Mining, Metallurgy and Chemical Engineering, Johannesburg, South Africa

ARTICLE INFO

Keywords:
CP-Ti
Spark plasma sintering
Pressure
Interstitial elements
Hardness

ABSTRACT

In this study the effect of sintering pressure on the densification, microstructure and mechanical properties of commercial pure titanium (CP-Ti) powders with varying chemistry was investigated. The sintering was performed at a constant dwell time of 3 min at varying temperature and pressure in the range of 550–900 °C and 25-75 MPa in vacuum, respectively. Full densification with high Vickers hardness values of 340 HV and 262 HV was obtained at 25 MPa at 800 °C and 900 °C respectively for two commercial powders with different average particles sizes. Different microstructural transformations with respect to increasing temperature and pressure were observed on the sintered pellets. The results were discussed emphasizing the huge role of the interstitial elements, contained in the starting powders, on the properties (relative density, Vickers hardness and microstructure) of the dense samples. This paper shows that good mechanical properties can be obtained by SPS technique when CP-Ti powders are sintered at very low temperature during a short period in contrast to conventional fabrication techniques.

1. Introduction

Titanium and its alloys are well-known throughout engineering applications for their combined desirable properties of high specific strength to weight ratio, low density, biocompatibility and relatively good corrosion resistance [1]. The production of bulk titanium involves expensive complex Kroll's processes such as refining, distillation and dissolution. These are performed using specific devices in a vacuum environment to avoid contamination by gaseous phases [2]. The resultant titanium product from the Kroll's process is then leached and a spongy titanium residue obtained is further processed [3]. Due to the high cost of production, these classes of materials are extensively used in high added value industries such as the aerospace and biomedical applications [4]. The crystal structure of high purity titanium from room temperature to 882 °C has a hexagonal closed packed (HCP) known as alpha (α) phase, above 882 °C it transforms into a body centred cubic (BCC) crystal structure, the beta (β) phase. The α-Ti and β-Ti have different densities of 4.51 g/cm^3 and 4.35 g/cm^3 respectively [1]. As a result of their light-weight coupled with moderately high strength and outstanding corrosion resistance properties, these have made titanium candidate material for other engineering applications such as automotive, offshore and energy industries [5]. For all of these reasons, focus has been on economical alternative production routes such as powder metallurgy techniques commonly by Hot Pressing (HP) and Spark Plasma Sintering (SPS), which are experiencing a renew of interest in recent years because they can allow to generate parts with complex shapes (Near Net Shape) [6] and then reduce the ratio between the cost of material purchased to the cost of the part.

In Hot Pressing (HP), a conventional sintering method, the powder is loaded into a graphite mold and sintered, under uniaxial applied pressure, by indirect heating via resistive heating units [7]. However, HP often requires very long time for sintering (several hours) and as a result high energy consumption. On the opposite, Spark Plasma Sintering (SPS) allows rapid consolidation (several minutes) and controlled grain growth by the reduction of the sintering temperature and time [8–10]. Here also the powder is loaded in a graphite mold and a uniaxial pressure is applied but the heating is directly obtained by the use of DC pulsed current passing through the material and/or the mold [11]. The two methods are widely used by researchers, SPS technique is a promising technique due to aforementioned reasons [12]. Ti6Al4V master alloy and TiAl intermetallics are among advanced materials that are widely used in high added value industries and thus most investigated by the economic SPS technique [13–20] while only few investigations are focused on SPS of CP-Ti.

* Corresponding author at: CIRIMAT, Université de Toulouse, CNRS, Université Toulouse 3 - Paul-Sabatier, 118 route de Narbonne, 31062 Toulouse cedex 09, France.
E-mail address: glendamotsi5@gmail.com (G.T. Motsi).

https://doi.org/10.1016/j.powtec.2019.01.005

Sintering of CP-Ti by SPS has been reported by Zadra, et al. [4], Weston, et al. [20], Shon, et al. [21] and Shon, et al. [7]. In their studies, these authors have shown that sintered CP-Ti components produced have similar Vickers hardness values close to ASTM grades (126-265 HV) [1]. Zadra, et al. [4] investigated the use of SPS on 45 μm spherical CP-Ti grade 1 and irregular shaped CP-Ti grade 3. Sintering experiments were conducted in the temperature range 750–1100 °C for 5 min, under uniaxial pressure of 60 MPa in vacuum followed by free cooling to produce SPS pellets with diameter and thickness of 30 mm and 5 mm respectively. Full densification for both grades was reached at 950 °C but at 800 °C the relative density was already 99%. However, the grain sizes of the two grades were different when sintered at 950 °C. CP-Ti grade 1 grains were coarser (~30 μm) compared to that of CP-Ti grade 3 (~16 μm). These authors explained these differences by the amounts of dissolved oxygen which was measured on the sintered pellets and was relatively higher (~0.32 wt%) in CP-Ti grade 3 compared to CP-Ti grade 1 (~0.075 wt%). On the contrary, Weston, et al. [20] explained this phenomenon in terms of particles shapes. For spherical particles the grain growth was rapid because there were higher initial particle-to-particle contacts with smaller pores and thus underwent more densification. In contrary to areas with less particle interactions and larger pores as found in irregular shaped particles leading to lower densification. However, it is known that, oxygen is very detrimental to the mechanical properties of CP-Ti and its alloys because it has an influence on the microstructure [22]. ASTM CP-Ti grades are classified according to the oxygen content dissolved and this has shown to have effect on the transus temperature and Vickers hardness. For instance ASTM grade 1 has low oxygen content of 0.18 wt% (~126 HV) leading to lower transus temperature (890 °C) while grade 3 has high oxygen content of 0.35 wt% (~280 HV) thus increasing the transus temperature to 920 °C [1,2]. Zadra, et al. [4] found that Vickers hardness of CP-Ti grade 3 (~190-240 HV) was higher than CP-Ti grade 1 (~120-150 HV) whatever the sintering temperature. The difference in Vickers hardness was attributed to high amount (~0.3–0.34 wt%) of oxygen dissolved in grade 3.

Eriksson, et al. [23], studied the influence of sintering pressure and temperature on the morphology of SPS partially consolidated CP-Ti powders. The compacts heated to 200 °C and 500 °C with 50 MPa pressure did not present change in grain size and morphology but the latter sample at 600 °C was ~90% dense. According to the authors, at 500 °C, particles deformation features were observed at grain boundaries instead of micro-welding and local melting of particles. However, the authors seem not to discuss the effect of pressure on the sintering mechanisms occurring. Different sintering mechanisms influenced by compaction pressure have been reported for Ti6Al4V alloy during SPS [16]. The authors explained that sintering mechanisms at 5 MPa compaction pressure occurred by electric discharges between particles and were dominant during the whole sintering stage. At much higher compaction pressure, at 25 MPa and above, the electric discharges were only dominant in the early stages of sintering and were suppressed thereafter. The presence of spark discharges which is a pathway for electron migration have been proposed by Tokita [24]. This phenomenon occurs in the initial stages of sintering and leads to neck formations between particles. Experimentally neck f0ormations have been observed for Ti6Al4V alloy with and without applied pressure [25]. In contrast, Trzaska, et al. [26] have suggested no detection of the electric arcs, plasma or local overheating in TiAl intermetallic, but plastic deformation as the main densification mechanism.

Garbiec, et al. [16] further suggest that increased compaction pressure assisted in densification during heating by more rapid formation of necks favoring Joule effect which in turn enhanced diffusion and thereafter grain growth resulted. The grain sizes of samples sintered with heating rate of 300 °C/min increased from 15.49 ± 3.81 μm at 5 MPa to 143.6 ± 46.8 μm at 25 MPa. However at 50 MPa the grain sizes reduced to 86.94 ± 19.28 μm, authors explain that Joule effect was inferior at this pressure compared with 25 MPa. The same effect was observed for 200 °C/min and 400 °C/min heating rates. Wang, et al. [19] report plastic deformation as densification mechanism in TiAl intermetallics prepared by SPS, the authors related the effect of pressure on density. At sintering temperature of 1150 °C, by increasing pressure from 10 MPa to 50 MPa, the density gradually increased from 3.947 g/cm^3 to 3.967 g/cm^3. The authors explained that higher sintering pressure led to more severe plastic deformation and it accelerated the mass transport between the particles which promoted densification. Plastic deformation of particles was confirmed by Trzaska, et al. [26], TEM thin foils were extracted in between necks of sintered TiAl powder particles, high densities of dislocations and twins which are characteristics of plastic deformation were observed.

Despite the reported studies on the densification and mechanisms governed by sintering pressure for Ti6Al4V alloy and TiAl intermetallic, there is however limited literature on pressure effect on densification of CP-Ti powders. In the present work SPS technique is used to sinter CP-Ti powders and the effect of sintering pressure on densification, microstructure and mechanical properties are thoroughly investigated on two CP-Ti powders containing different amounts of interstitials.

2. Experiments procedure

2.1. Characterization of the raw materials

As-received CP-Ti powders with -325mesh size prepared by hydride dehydride process producing powders with angular morphology were sourced from PI-KEM Ltd., UK (Ti(S)) and CERAC incorporated, US (Ti (L)). The powders morphology were characterized by scanning electron microscope (SEM) JSM6510LV and the particle sizes distribution (PSD) was determined using Mastersizer 3000 in dry conditions. Interstitial elements O, H, N and C were analyzed by instrumental gas analysis technique at TIMET, Fr using LECO ONH836 and LECO CS844 respectively. The iron content was analyzed at Marion Tech. using ICP-AES technique. Phases present were identified by using D4-Endeavor X-ray diffractometer by Bruker with monochromatic Cu Kα radiation at 40KV and 40 mA. The diffraction patterns were initially recorded in 2Θ range 10–100° at step size of 0.01569, then it was found that the interesting section in the patterns was in between 34 and 42° the diffraction was then done at this range at a much lower step size of 0.00998. The phases present were identified by searching and matching of peak positions and intensities with those in JCPDS using EVA software.

2.2. Spark plasma sintering

The CP-Ti powders were spark plasma sintered using a Dr. Sinter 2080 unit, SPS Syntex Inc., Japan, available at Plateforme Nationale de Frittage Flash located at the Université Toulouse 3 Paul Sabatier, using Ø8mm Graphite die (Gr die) lined with a 0.2 mm graphite paper (PERMA-FOIL®Toyo Tanso). The sintering was performed at varying temperatures and uniaxial applied pressure in the range of 550 °C–900 °C and 25 MPa–75 MPa respectively. A constant holding time and heating rate of 3 min and 100 °C/min was used. K-type thermocouple was inserted 3 mm in depth of the Gr die to monitor all temperature readings. To ensure a uniform initial compaction for all the powders, pre-compaction at 25 MPa for 3 min was performed prior the start of the thermal cycle. After sintering completion, the pellets were removed from the Gr die and the graphite adhered to the sintered pellets was removed by grinding using P320 SiC paper. Thereafter the relative density was measured by using Archimedes principle using a hydrostatic balance (Sartorius MSE224S-YDK03) and geometrically (when the sample densification was lower than 92%). In SPS the temperature distribution is known to differ. Especially the temperature within a conductive powder is normally higher than the one measured on the graphite die [27]. Therefore, experiments were performed to measure the real temperature in the powder and to determine temperature difference between Gr die and CP-Ti powder using K-type thermocouples.

Gr dies with Ø8 and Ø20 diameters were used, a hole was drilled through Gr die reaching maximum thickness (16.6 and 29.6 mm respectively) and then the thermocouple was inserted through reaching CP-Ti powder filled inside Gr die. The second thermocouple was inserted as normal (3 mm in depth) on the Gr die. The set-point temperature was 800 °C and 25 MPa pressure was used at constant heating rate of 100 °C/min with a dwelling time of 3 min.

2.3. Mechanical properties

The sintered pellets were cold mounted using epoxy resin and the surface was grounded using a series of SiC papers P320, P600, P1200 and P2400. Then final polishing with colloidal silica on a neoprene cloth for a minimum of 10 min was performed to produce a scratch free surface. Vickers hardness was then determined using a HM-200 Mitutoyo hardness tester on the polished pellets at a load of 0.5 kg and nine indentations were made in different sections of the pellets.

2.4. Microstructure

Chemical etching was done for 15 s to reveal the microstructure using Kroll's etchant consisting of 92 ml distilled water, 6 ml of nitric acid and 2 ml hydrofluoric acid. The etched sintered pellets were thoroughly rinsed with tap water to remove any traces of the etchant and then hot dried. The microstructure was observed and analyzed using a SEM (JSM6510LV). The volume fraction of secondary α-phase was quantified with ImageJ software.

3. Results and discussion

3.1. Characterisations of the starting powders

Particles morphology of the CP-Ti powders is shown in Fig. 1. It was observed from the SEM micrographs that the powders particles were irregular shaped but the periphery for CP-Ti with smaller particles (Ti(S)) was sharper while that of CP-Ti with larger particles Ti(L) was a bit smoother. The PSD analysis of the received powders show that Ti (S) had a larger particle sizes distribution than Ti(L). The average particles size of Ti(S) (D_{50} = 25,9 μm) was smaller than that of Ti(L) powder (D_{50} = 35,9 μm). Although the morphology of the two powders was similar, elemental analysis (Table 1) revealed significant differences in compositions. Ti(S) had high oxygen content (7315 ppm) but with low hydrogen content (546 ppm), whereas Ti(L) had high hydrogen content (2226 ppm) and low oxygen content (2451 ppm). A high iron content of 298 ppm was analyzed in Ti(S) while it was lower in Ti (L) with 25 ppm. In the XRD pattern shown in Fig. 2, both Ti powders were identified by HCP α-Ti phase while TiH_2 lines were also detected for Ti(L). The presence of the hydride phase in the latter powder can

Table 1
Interstitial elements content (ppm), determined using instrumental gas analysis.

	C	H	N	O	Fe[a]
Ti(S)	205	546	175	7315	298
Ti(L)	125	2226	326	2451	25

[a] ICP-OES.

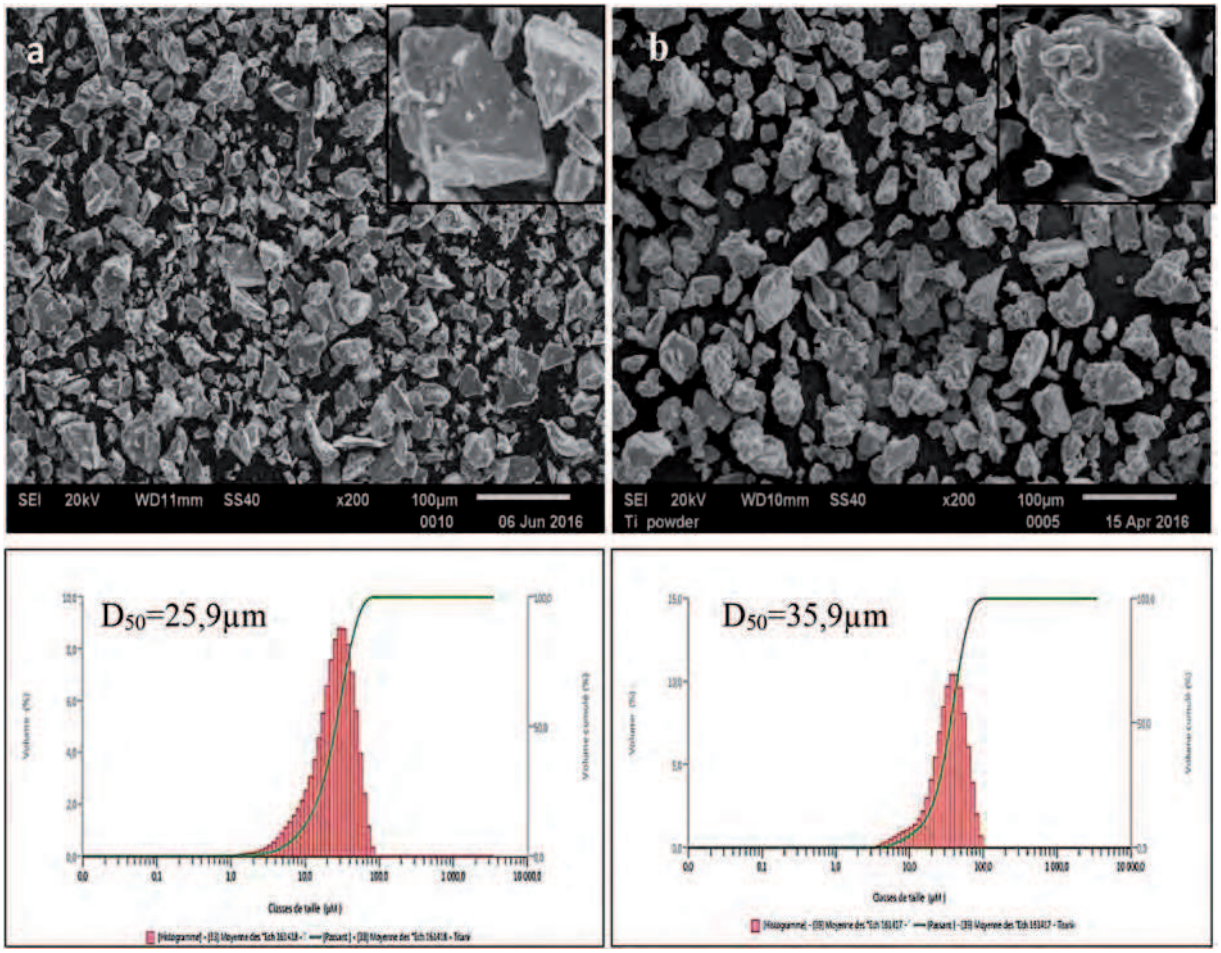

Fig. 1. SEM micrographs of -325mesh powders and their respective PSD analysis, a: Ti(S) and b: Ti(L).

result from an incomplete removal of hydrogen during processing, especially since hydrogen is present in high amount compared to Ti(S) (Table 1).

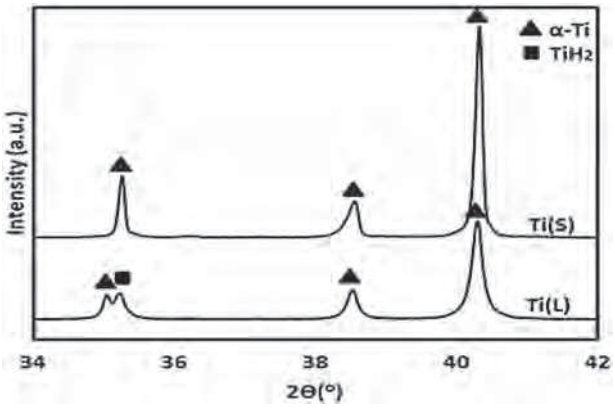

Fig. 2. XRD pattern of as-received powders.

3.2. Temperature variation during sintering

The temperature difference between Gr die and powder was measured in Ø8mm and Ø20mm. Fig. 3 shows the temperature difference in the two measured locations. It was observed that the temperature increased linearly with time for the two locations. A variation in temperature was observed from 240 s until final stages of the sintering cycle. The overall temperature measured in the powder was approximately 8% higher than in the Gr die. For Ø8mm Gr die in Fig. 3(a), it was found that when ramping up to reach the set-point temperature of 800 °C the temperature overshoot to 807 °C then stabilized to 800 °C at dwelling time. A similar behaviour was observed for Ti powder but higher temperatures were obtained in powder than in Gr die. Higher temperature of 874 °C was reached before dwelling which thereafter lowered to 868 °C just below 882 °C α to β-Ti theoretical transus temperature. Hence, the temperature difference just before and after dwelling was 67 °C and 68 °C respectively. In comparison, for a Ø20mm Gr die, much higher temperatures of approximately 10% exceeding the theoretical transus temperature were reached. Temperature difference of 97 °C and 89 °C before and after dwelling were recorded (see Fig. 3(b)). Fig. 3(c) further shows that temperature of CP-Ti powder in Ø20mm Gr die was approximately 21 °C higher than powder in Ø8mm Gr die. The temperature difference measured

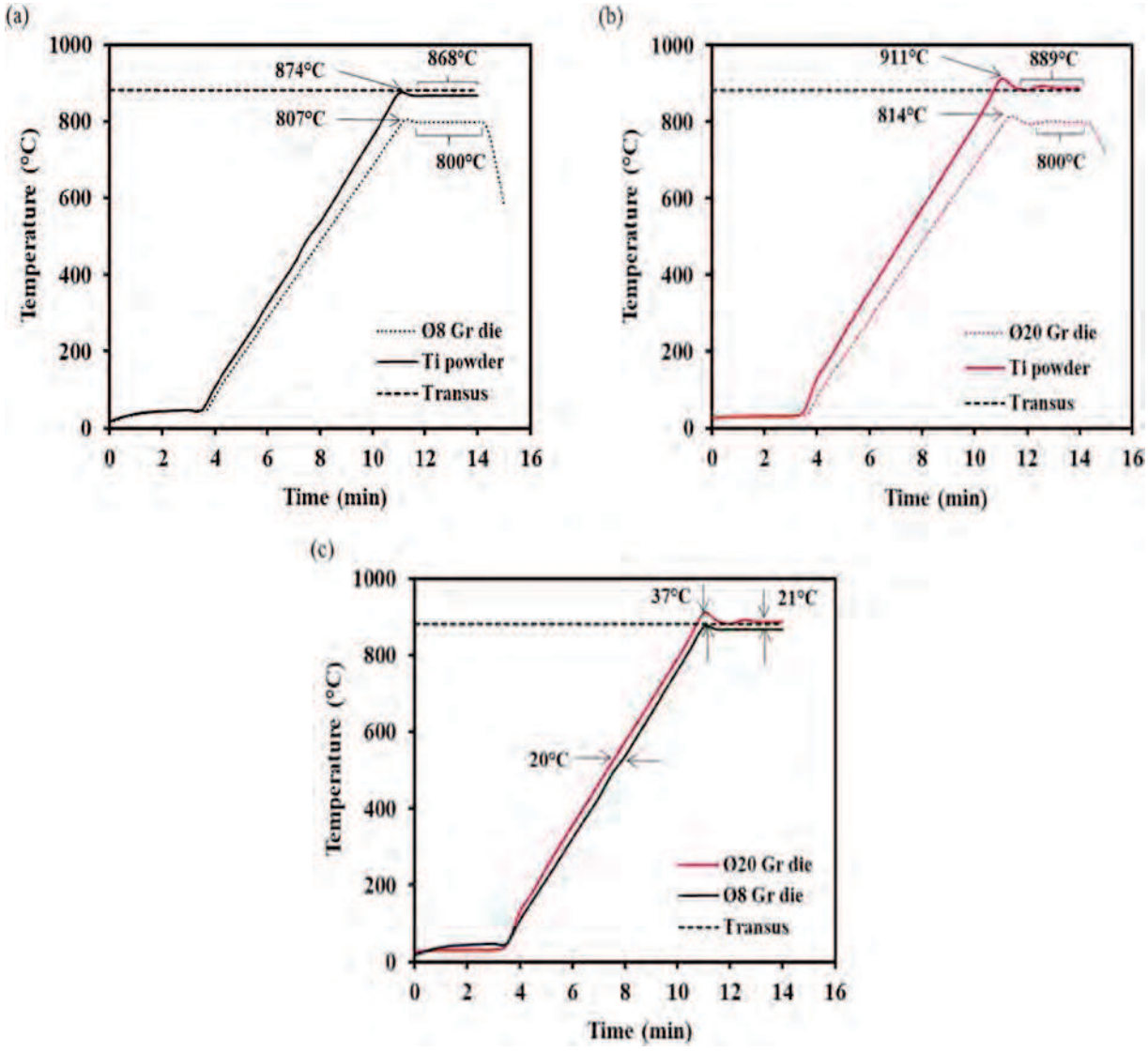

Fig. 3. Temperature difference between Gr die and Ti powder, a: Ø8 Gr die, b: Ø20 Gr die and c: Temperature difference between Ø8 and Ø20 Gr dies.

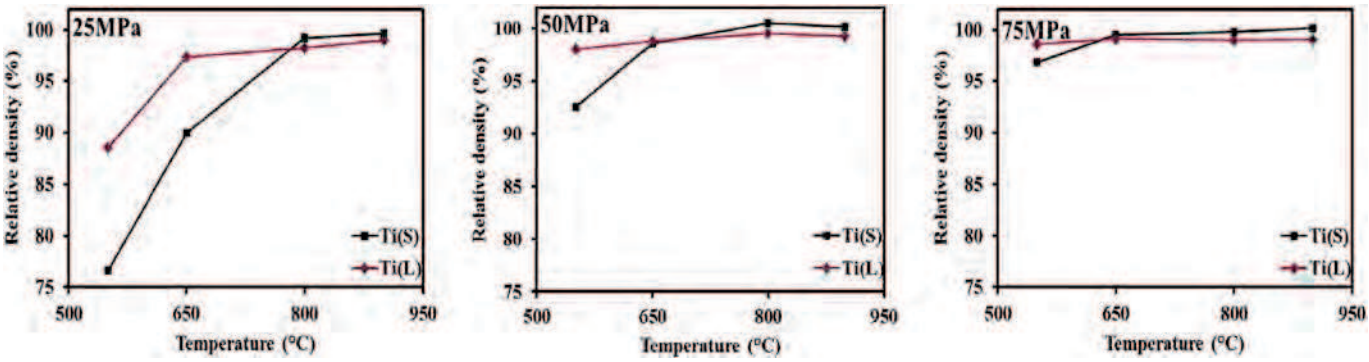

Fig. 4. Evolution of the relative density versus set-point temperature for three applied pressure a:25, b:50 and c:75 MPa for Ti(S) and Ti(L) SPS pellets.

between CP-Ti (1041 °C) and Gr die (1010 °C) reported in Matsugi, et al. [28] was 31 °C. Temperature measurements depend on the location of the thermocouple, in Matsugi, et al. [28] the thermocouple was positioned 2 mm from the internal diameter and in this study it was positioned 3 mm from the outer diameter. Hence with temperature gradient decreasing from the powder to the surface of the Gr die the temperature difference in Matsugi, et al. [28] was lower than in the present study.

3.3. Effect of sintering temperature and pressure on densification

Fig. 4 shows the variation of relative density for Ø8mm SPS pellets with the sintering temperatures for both Ti(S) and Ti(L). A density of 99% for Ti(S) and Ti(L) was reached at pressure of 25 MPa at 800 °C and 900 °C respectively. Further, as expected densification above 95% is reached at much lower temperatures as the applied pressure (75 MPa) is increased. Comparing to the alloy Ti6Al4V [16] full densification was reached at 1000 °C with higher heating rate of 300 °C/min and that of intermetallic TiAl [14] obtained at 950 °C in similar SPS conditions. More surprising, at 550 °C and 650 °C for 25 MPa the densification of Ti(S) pellets was expected to be higher than Ti(L) because of the small particles sizes. However, early microstructural transformation of Ti(L) due to high amount of hydrogen lowering the transus temperature promoting diffusion of atoms resulted in faster densification. This effect was also noticed at the respective increasing pressures at 550 °C for Ti(L). This indicated that for Ti(S) with high amount of dissolved oxygen increased the transus temperature thus limiting atoms diffusion for enhancing densification at lower temperatures.

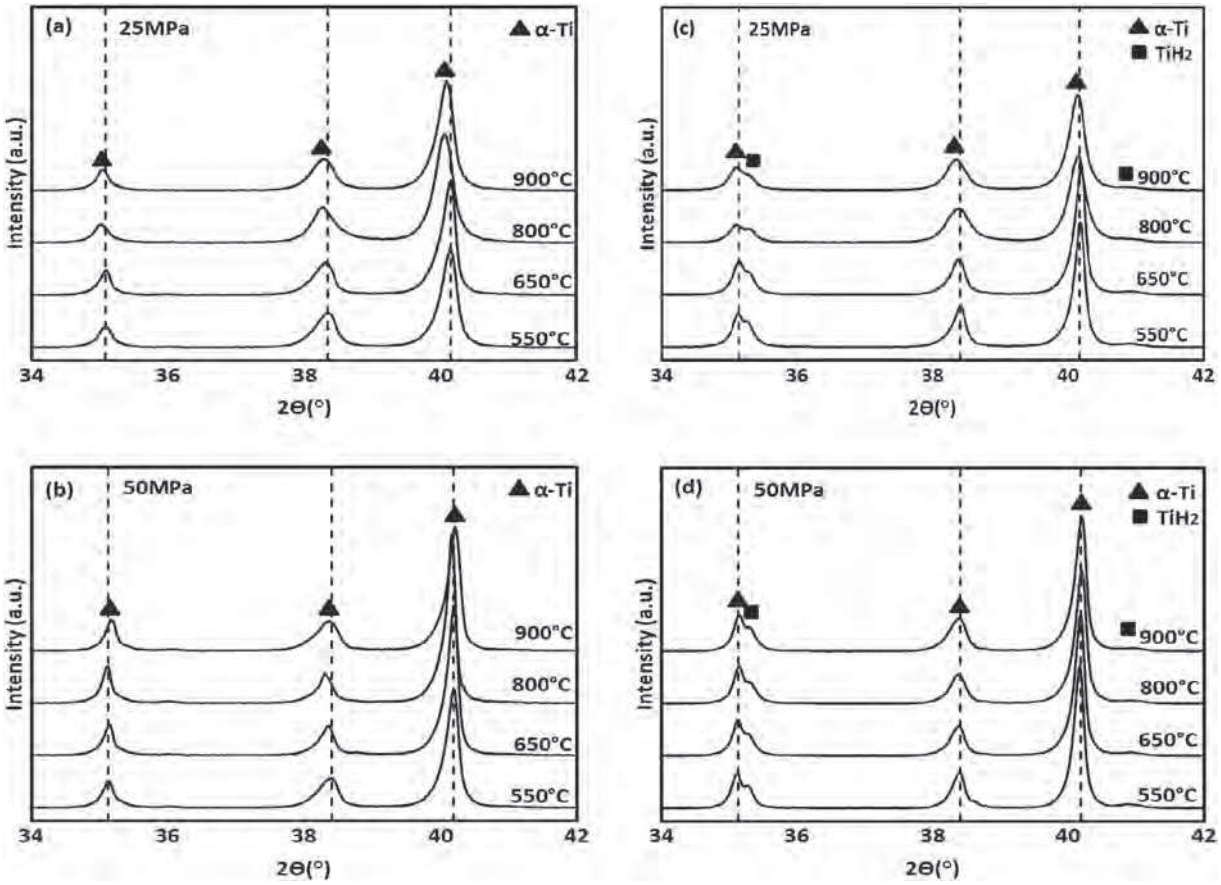

Fig. 5. Effect of temperature on the structure of SPS pellets at 25 MPa and 50 MPa for Ti(S) (a and b) and Ti(L) (c and d).

3.4. Effect of sintering temperature and pressure on the microstructure

XRD patterns of Ø8mm SPS pellets sintered at various temperatures is shown in Fig. 5. No specific effect is observed since all the XRD patterns of the pellets are similar to those of the starting powders. Except the slight negative and positive 2-theta shift observed when temperature and pressure were increased respectively. In the Ti(S) structure at 25 MPa shown in Fig. 5(a), the 2-theta angle slightly shifts to the left with increasing temperature, indicating that the lattice parameters are increasing and thus unit cell expansion. The negative 2-theta shift was however negligible at 50 MPa and also for Ti(L) in Fig. 5 (c and d). Fig. 6 shows the effect of applied pressure on the structure of the sintered pellets. In Fig. 6(a) for Ti(S) at lower temperature of 650 °C with increased pressure there was a negligible positive shift of 2-theta angle, this behaviour was however not observed for Ti(L) see Fig. 6(c). For a temperature of 900 °C in Fig. 6(b), the positive shift of 2-theta angle was more pronounced for 50 MPa than 75 MPa, as for Ti(L) in Fig. 6(c and d) the shift was negligible. Comparing Ti(S) and Ti(L), the lattice parameters for Ti(S) are reduced with the change in pressure at all temperatures but for Ti(L) the change is negligible under the same conditions.

Microstructural evolution of Ti(S) sintered pellets with increasing temperatures and pressure is presented in Fig. 7. Porosity was observed at low temperatures of 550 °C and 650 °C, with the respective pressure and this was in good agreement relative density evolution reported in Fig. 4. As previously discussed for varying temperature in the Gr die and powder, the actual temperature of the powder was higher than set-point temperature. In this discussion, we considered the actual temperature of the sample to be in excess of 68 °C. Microstructural transformation of Ti(S) at 800 °C and 25 MPa when cooling from above beta phase transus temperature, show nucleation and growth of secondary α-phase (α_s) identified as the brighter phase at the grain boundaries of primary α-phase (α_p) which was identified as the darker phase [2]. This could indicate that α_s-phase nucleation is initiated in the temperature range 718 °C - 868 °C, with few degrees below the α to β-Ti transus temperature for high purity titanium. When temperature was further increased to 900 °C the microstructure transformed into equiaxed like structure, with increased volume fraction (21%) of α_s-phase. It was also observed that by increasing pressure to 50 MPa at 800 °C, an increase in the volume fraction (76%) of α_s-phase was noticed and decreased at 75 MPa (19%). This was however not observed at 900 °C, only the equiaxed like structure for α_s-phase became well defined. Microstructural evolution of Ti(L) is shown in Fig. 8, when the temperature was increased to set-point of 800 °C the microstructure completely transformed to lamellar structures with coarser α_s-phase, which was very visible as the pressure was increased to 50 MPa. The pressure effect on the lamellar structure and α_s-phase volume fraction was minimal (insignificant phase shift as revealed by the diffraction patterns in Fig. 6). Nucleation and growth of α_s-phase seem to have occurred at much lower temperatures of 618 °C in the Ti(L) as compared with Ti(S).

For the two powders investigated the dominant phases present were α_p and α_s-phases because there were few β-phase stabilising elements. When CP-Ti is heated to the β-Ti region and cooled down to α-Ti region, β-Ti phase is present only in small quantities or not retained and the structure transforms back to its room temperature α-Ti phase. Microstructure by diffusion controlled nucleation and growth is obtained by slower cooling rates producing a coarse Widmanstätten-α plus α-prime as observed for Ti(L).

Microstructural transformation for Ti(S) and Ti(L) at 800 °C at the various pressures is presented in Fig. 9. The morphology of α_s-phase in the two samples was different at all pressures. At 25 MPa, Ti(S) has a combination of needle-like and irregular-shaped α_s-phase. When

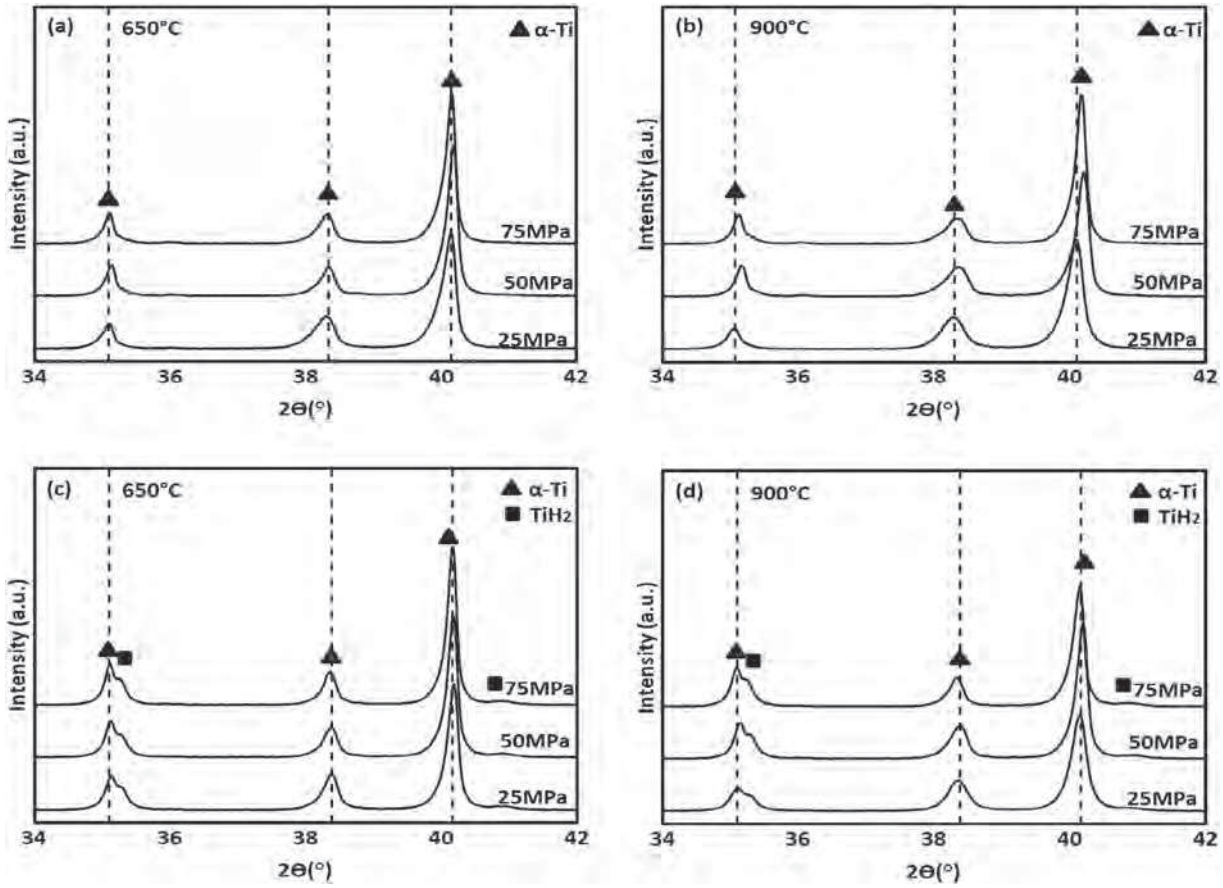

Fig. 6. Effect of pressure on the structure of SPS pellets Ti(S) a: 650 °C, b: 900 °C and Ti(L) c: 650 °C and d: 900 °C.

pressure was increased to 50 MPa α_s-phase grain size increased then reduced at 75 MPa. Ti(L) at 25 MPa has elongated needle-like and thickened α_s-phase showing the formation of lamellar structure. The lamellar structure is clearly visible at 50 MPa and 75 MPa for Ti (L) where the grain sizes slightly increased. These observations indicate that Ti(S) microstructure transformation was delayed due to the high amount of dissolved oxygen (Table 1) which stabilized the α_p-phase. On the contrary, high amount of beta phase stabiliser hydrogen was measured in Ti(L) (Table 1), promoting early microstructure transformation.

Moreover, on the grain growth with increase in pressure it appeared that different mechanisms occur during sintering and this phenomenon was more visible for Ti(S). At low pressure of 25 MPa the dominant mechanism could be due to electric discharging and neck formations between particles. This occurred by spark discharging between particles whereby high temperatures are reached causing vaporization and melting at the particles surface. This transient phenomenon resulted in necks formation around the contact area between the particles. The necks gradually developed and plastic deformation progressed during sintering until full densification was reached [24]. However, at high pressures these mechanisms were only dominant in the early stages of sintering. At high sintering pressure of 50 MPa and 75 MPa the possible mechanisms occurred were electric discharges dominant only in the beginning of sintering and were suppressed after. Particles rapidly plastically deformed and rapid neck formation occurred in favor of the Joule effect which enhanced diffusion and the consequent grain growth. Hence sintering occurred by mechanical mechanisms in contrast to low sintering pressure [16].

3.5. Effect of sintering temperature and pressure on vickers hardness

Hardness evolution with increasing temperature and pressure for Ti(S) and Ti(L) is shown in Fig. 10. The hardness of Ti(S) at 25 MPa increased as the temperature was increased from 550 °C to 800 °C then

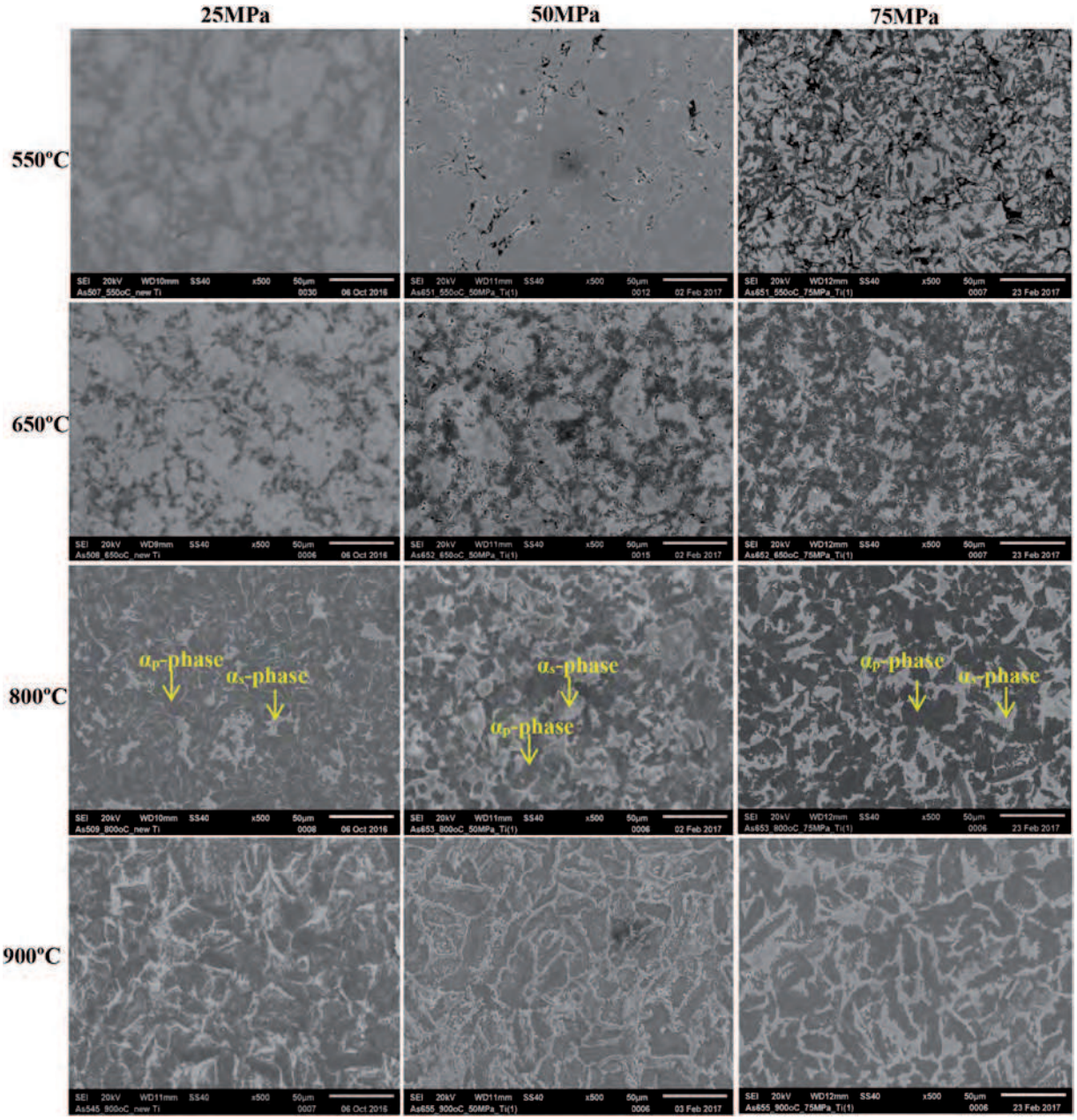

Fig. 7. SEM micrographs of Ti(S) SPS pellets.

decreased after at higher temperatures. This could be due to the 21% volume fraction of α_s-phase formed at 900 °C, in contrast to 12% at 800 °C. The same behaviour is observed at 75 MPa. Whereas Ti (L) hardness increases with increasing temperature and pressure. It seems that Ti(L) present the same hardness, whatever the applied pressure. The plateau was reached at lower temperature as the pressure was increased. There was a significant difference in hardness values for Ti (S) and Ti(L) SPS pellets, the values are in between 102 and 340 HV and 160-260 HV respectively, in agreement with values of the literature [1,21]. The highest hardness of 340 HV was obtained at 25 MPa and 800 °C for Ti(S) with a "needle-like" microstructure consisting of low volume fraction of α_s-phase as shown in Fig. 9(a), and that of Ti(L) with lamellar microstructure in Fig. 9(f) was 262 HV at 25 MPa and 900 °C. The high hardness of Ti(S) was attributed by the smaller particle sizes (25.9 μm) (according to Hall-Petch) [29] and the high amount of oxygen dissolved in the matrix delaying the structural transformation into a lamellar structure with low mechanical properties. These results are similar to those reported by [21], who reported that CP-Ti with 25.06 μm particles sizes with highest oxygen content yielded high hardness, tensile strength and reduced ductility, as opposed to 86.368 μm powder. Zadra, et al. [4] investigated the dependence of mechanical properties on oxygen content by investigating CP-Ti powders of the same particles size of 45 μm but different oxygen contents. Their results also demonstrated the same effect of oxygen on mechanical properties agreeing with the present study.

The Vickers hardness was plotted as a function of the relative density (Fig. 11). SPS pellets with highest relative density have high hardness and vice versa **[30]**. The effect of pressure on densification is observed, the relative densities are in the range 77–100%, 93–100% and 97–100% for 25 MPa, 50 MPa and 75 MPa respectively. However, the increased

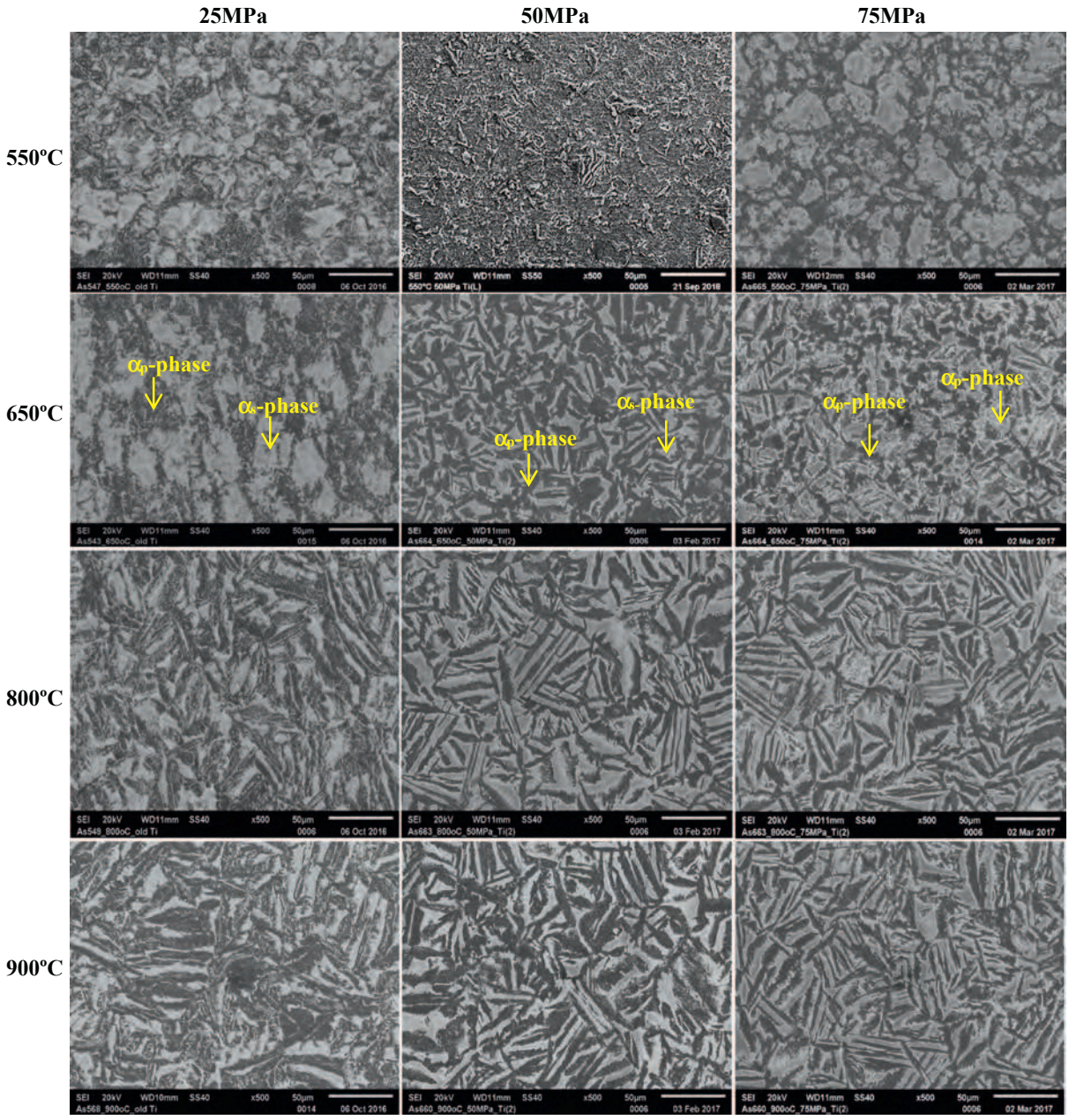

Fig. 8. SEM micrographs of Ti(L) SPS pellets.

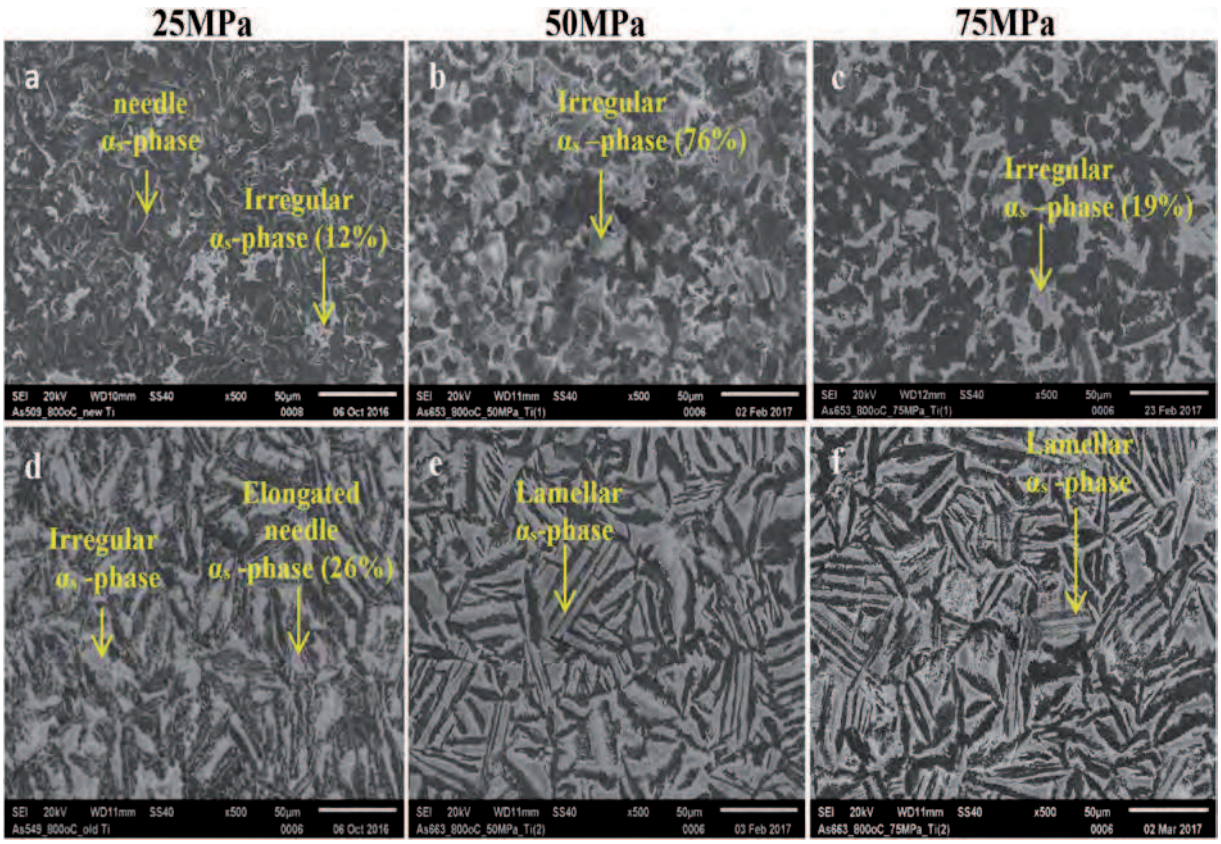

Fig. 9. SEM micrographs for microstructure transformation at 800 °C and varying pressures of 25-75 MPa, Ti(S) (a, b & c), Ti(L) (d, e & f).

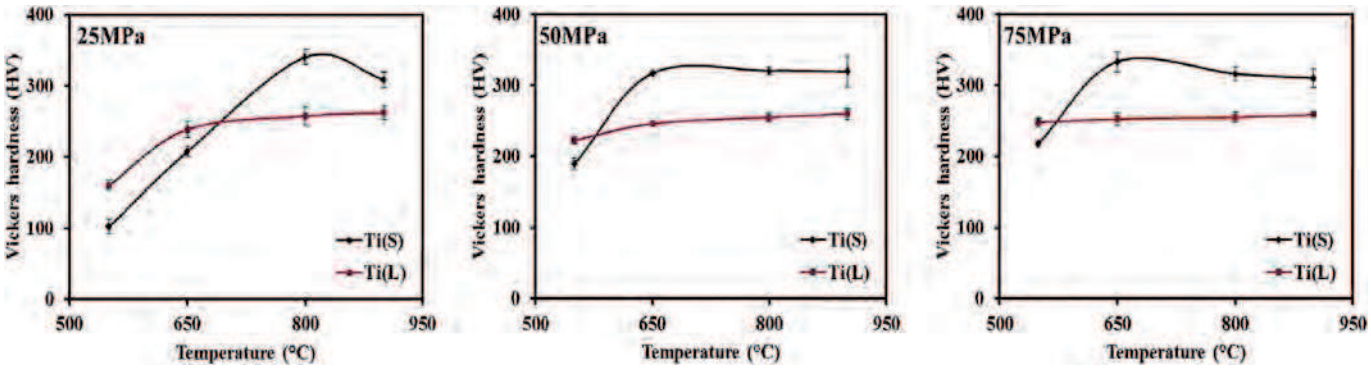

Fig. 10. Vickers hardness vs temperature at 25 MPa, 50 MPa and 75 MPa for Ti(S) and Ti(L) SPS pellets.

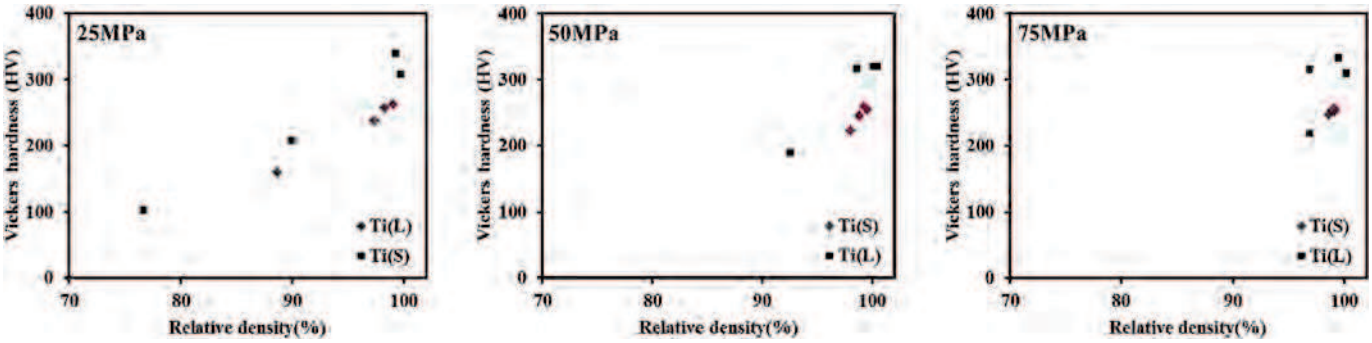

Fig. 11. Vickers hardness vs relative density at 25 MPa, 50 MPa and 75 MPa for Ti(S) and Ti(L) SPS pellets.

applied pressure shows to have minor effect on the hardness of the SPS pellets especially for those sintered at high temperatures (800–900 °C) the values obtained are almost in the same range.

4. Conclusions

Sintered CP-Ti samples were obtained at temperatures ranging from 550 to 900 °C from CP-Ti powders of different composition. Full densification was obtained at 25 MPa at temperatures of 800 °C and 900 °C for Ti(S) and Ti(L) respectively. The microstructure transformation for Ti (S) with high amount of oxygen was delayed and only started at higher temperatures. As for Ti(L) with high amount of hydrogen the transformation was promoted at very low temperatures and increased pressure. As found in literature oxygen is α-phase stabiliser raising the α to β transus temperature while hydrogen is a β-phase stabiliser lowering the transus temperature. The different elemental composition of the fully dense samples resulted in different microstructures formation with Ti(S) characterized by needle like structure and for Ti(L) lamellar structure was obtained. Thus Ti(S) exhibited higher Vickers hardness of 340 HV compared to Ti(L) with 262 HV. In addition, smaller particles size resulting in retention of small grains for Ti(S) also contributed to the high Vickers hardness value obtained in comparison to Ti(L). It was found that increase of α_s-phase volume fraction with pressure could be related to electric discharges between particles and plastic deformation of particles at low and high pressure respectively. Increment of α_s-phase volume fraction was found to be influenced by increased pressure, temperature and high amount of hydrogen.

Data statement

Data for the submitted manuscript cannot be provided during paper submission because it is part of ongoing research

Acknowledgements

Special thanks to the AESOP+ project for the PhD grant (20140878) and TIMET, Fr for their generosity with analyzing interstitials elements in the powders.

References

[1] G. Welsch, R. Boyer, E. Collings, Materials Properties Handbook: Titanium Alloys, ASM international, 1993.
[2] G. Lütjering, J.C. Williams, Engineering materials and processes: titanium 8 (2007) 1–16.
[3] M.J. Donachie, Titanium: A Technical Guide, ASM international, 2000.
[4] M. Zadra, F. Casari, L. Girardini, A. Molinari, Powder Metall. 51 (2008) 59–65.
[5] C. Leyens, J. Hausmann, J. Kumpfert, Adv. Eng. Mater. 5 (2003) 399–410.
[6] C. Manière, E. Nigito, L. Durand, A. Weibel, Y. Beynet, C. Estournès, Powder Technol. 320 (2017) 340–345.
[7] J.-h. Shon, J.-m. Park, K.-s. Cho, J.-k. Hong, N.-k. Park, O.H. Myung-hoon, Trans. Nonferrous Metals Soc. China (2014) 24.
[8] R. Chaim, M. Levin, A. Shlayer, C. Estournès, Adv. Appl. Ceram. 107 (2008) 159–169.
[9] R. Chaim, R. Marder, C. Estournés, Z. Shen, Adv. Appl. Ceram. 111 (2012) 280–285.
[10] R. Orru, R. Licheri, A.M. Locci, A. Cincotti, G. Cao, Mater. Sci. Eng. 63 (2009) 127–287.
[11] Z.A. Munir, U. Anselmi-Tamburini, M. Ohyanagi, J. Mater. Sci. 41 (2006) 763–777.
[12] Y. Yang, M. Qian, Spark Plasma Sintering and Hot Pressing of Titanium and Titanium Alloys, Titanium Powder Metallurgy: Science, Technology and Applications, Butterworth-Heinemann, 2015.
[13] M. Abedi, D.O. Moskovskikh, A.S. Rogachev, A.S. Mukasyan, Metall. Mater. Trans. B Process Metall. Mater. Process. Sci. 47 (2016) 2725–2731.
[14] A. Couret, G. Molénat, J. Galy, M. Thomas, Intermetallics 16 (2008) 1134–1141.
[15] K. Crosby, L.L. Shaw, C. Estournes, G. Chevallier, A.W. Fliflet, M.A. Imam, Powder Metall. 57 (2014) 147–154.
[16] D. Garbiec, P. Siwak, A. Mróz, Arch. Civ. Mech. Eng. 16 (2016) 702–707.
[17] D. Martins, F. Grumbach, C. Manière, P. Sallot, K. Mocellin, M. Bellet, C. Estournès, Intermetallics 86 (2017) 147–155.
[18] K. Matsugi, N. Ishibashi, T. Hatayama, O. Yanagisawa, Intermetallics 4 (1996) 457–467.
[19] D. Wang, H. Yuan, J. Qiang, Meta 7 (2017) 201.
[20] N.S. Weston, F. Derguti, A. Tudball, M. Jackson, J. Mater. Sci. 50 (2015) 4860–4878.
[21] J. Shon, I.-B. Song, K.-S. Cho, Y.-i. Park, J.-K. Hong, N.-K. Park, M.-H. Oh, Int. J. Precis. Eng. Manuf. 15 (2014) 643–647.
[22] M. Yan, W. Xu, M.S. Dargusch, H.P. Tang, M. Brandt, M. Qian, Powder Metall. 57 (2014) 251–257.
[23] M. Eriksson, Z. Shen, M. Nygren, Powder Metall. 48 (2005) 231–236.
[24] M. Tokita, Proceeding of NEDO International Symposium on Functionally Graded Materials, Japan, 1999 22.
[25] U. Kus, Science et Génie des Matériaux, Université Toulouse III - Paul Sabatier, Toulouse, France, 2017 249.
[26] Z. Trzaska, A. Couret, J.-P. Monchoux, Acta Mater. 118 (2016) 100–108.
[27] U. Anselmi-Tamburini, S. Gennari, J.E. Garay, Z.A. Munir, Mater. Sci. Eng. A 394 (2005) 139–148.
[28] K. Matsugi, H. Kuramoto, O. Yanagisawa, M. Kiritani, Mater. Sci. Eng. A 354 (2003) 234–242.
[29] W.D. Callister, D.G. Rethwisch, Materials Science and Engineering, John Wiley & Sons NY, 2011.
[30] A. Miklaszewski, D. Garbiec, K. Niespodziana, Adv. Powder Technol. 29 (2018) 50–57.